Available online at www.sciencedirect.com
ScienceDirect
Cement & Concrete Composites 29 (2007) 490–497
Cement & Concrete Composites
www.elsevier.com/locate/cemconcomp

Simultaneous measurement of shrinkage and temperature of reactive powder concrete at early-age using fibre Bragg grating sensors

Allan C.L. Wong [a,*], Paul A. Childs [a], Richard Berndt [b], Tony Macken [b], Gang-Ding Peng [a], Nadarajah Gowripalan [b]

[a] School of Electrical Engineering and Telecommunications, University of New South Wales, Sydney, NSW 2052, Australia
[b] School of Civil and Environmental Engineering, University of New South Wales, Sydney, NSW 2052, Australia

Received 19 July 2006; received in revised form 1 February 2007; accepted 8 February 2007
Available online 27 February 2007

Abstract

The physical properties of reactive powder concrete (RPC) at early-age, i.e., the first 24 h from casting, and up to an age of 7 days is investigated experimentally using fibre Bragg gratings (FBGs), a type of fibre-optic sensors. A number of FBG sensors are multiplexed together and embedded directly into the RPC specimens, and the shrinkage and temperature change are measured directly and simultaneously. The final setting time and specimen size effect were also investigated. Results showed that there is an interplay between the shrinkage and temperature. The overall shrinkage for 7 days is 488 με, with the early-age shrinkage contributing about 77% of this. The temperature curve exhibits a double peak behaviour, with the first peak appears at about 7 h, which is the final setting time. There is a size effect in that smaller prisms have a higher overall shrinkage and lower temperature change than larger prisms.

Keywords: Fibre-optic sensor; Fibre Bragg grating; Reactive powder concrete; Early-age shrinkage; Temperature; Ultra-high strength concrete

1. Introduction

Reactive powder concrete (RPC) is a relatively new type of ultra-high strength concrete first introduced in 1994 [1,2]. It offers many advantages over normal strength and high performance concretes in terms of mechanical and composite properties, most notably: (i) ultra-high compressive strength (200–800 MPa); (ii) high flexural strength (up to 40 MPa); (iii) high ductility through the inclusion of short steel-fibre reinforcement; (iv) lightweight and (v) increased homogeneity because of the elimination of coarse aggregates. To date, the physical characteristics of RPC at early-age (the first 24 h from casting and may extend up to 7 days), in particular the early-age shrinkage, is still not well understood, despite the fact that it has been used in the construction of pedestrian and road bridges [3–5]. This is partly due to the relatively short history of RPC, and partly due to the practical difficulties in carrying out experiments while it is still in the plastic stage. In fact, the latter is the main problem in investigating the early-age physical properties of any type of concrete. For example, conventional methods, such as using electrical and mechanical strain gauges, of measuring the shrinkage of fresh RPC failed, mainly because no gauge-points could be established before the RPC is hardened. Indirect methods to derive and predict the early-age properties have been used. They are mainly based on calorimetric measurement [6–8], ultrasonic measurement [6–11], and hydrostatic weighing [6,7,9] of the specimen. They require complicated and delicate experimental setups, and the use of indirect quantities such as the degree of hydration, dissipated heat power, shear and compressive waves and their velocities, and weight change, in order to deduce the mechanical properties. In these methods the actual shrinkage has still not been directly measured.

* Corresponding author. Tel.: +61 2 93855534.
E-mail addresses: allan.wong@unsw.edu.au (A.C.L. Wong), G.Peng@unsw.edu.au (G.-D. Peng), N.Gowripalan@unsw.edu.au (N. Gowripalan).

0958-9465/$ - see front matter © 2007 Elsevier Ltd. All rights reserved.
doi:10.1016/j.cemconcomp.2007.02.003

At early-age, the main types of shrinkage of RPC are autogenous, thermal and drying shrinkages. Although some other shrinkages, such as carbonation shrinkage, are also present, they contribute very little to the overall shrinkage at early-age and may be neglected. Early-age shrinkage leads to surface cracks and the formation of early-age cracks that would extend further at later stages. Since the RPC undergoes rigorous chemical reactions and phase transitions during the early-age, a knowledge of the physical characteristics at this period provides useful information and experimental data for the study of its deformation, the cause and severity of plastic shrinkage, swelling and early-age cracking. Also, it would be helpful for the improvement in the mix design and the choice of mixing materials.

Thus far, there have been only a few investigations of early-age shrinkage using fibre-optic sensors. These include the use of Fabry–Perot interferometers [12], low-coherence interferometry [13], and packaged fibre Bragg gratings (FBGs) [14] on cement paste [14] and unspecified types of concrete [12,13]. None of them were tested on RPC or on the simultaneous measurement of shrinkage and temperature. In this paper, the physical properties of RPC at early-age is being investigated experimentally using a technique based on FBGs, a type of fibre-optic sensors. The technique is capable of multiplexing a number of sensors, as well as taking all measurements automatically, continuously and remotely. The FBG sensors are embedded directly into the RPC specimens, and because of their small size, they are non-invasive to the specimens. The shrinkage and temperature change are obtained simultaneously, immediately after casting and up to an age of 7 days. In addition, the final setting time and the specimen size effect are investigated. The former is determined from the temperature characteristic, while the latter is performed by comparing specimens of two different sizes. It is hoped that by employing this technique, it would contribute to a better understanding of this ultra-high strength concrete at early-age, as well as offering a better and simpler experimental method in concrete research.

2. Measurement scheme

2.1. FBG sensing technique

An FBG is a type of fibre-optic device which consists of a periodic modulation of the core refractive index along the length of an optical fibre. The grating region can be used as a sensing element, and the typical grating length is about 5–20 mm. Thus, the FBG is considered as a point sensor similar to an electrical strain gauge. The FBG is specified by its characteristic wavelength called the Bragg wavelength, which is given by $\lambda_B = 2n_{eff}\Lambda$, where n_{eff} is the effective refractive index and Λ is the grating period. The shift in the Bragg wavelength due to strain ε and temperature T changes is given by [15]

$$\Delta\lambda_B = (1-p_e)\lambda_B\Delta\varepsilon + (\alpha+\xi)\lambda_B\Delta T, \tag{1}$$

where $p_e = (n^2/2)[P_{12} - \mu(P_{11}+P_{12})] \approx 0.22$ is the effective photoelastic coefficient, P_{ij} are the Pockels coefficients of the strain-optic tensor and μ is Poisson's ratio. $\alpha = (d\Lambda/dT)/\Lambda$ is the coefficient of thermal expansion, and $\xi = (dn_{eff}/dT)/n_{eff}$ is the thermo-optic coefficient. Both p_e and ξ are wavelength dependent due to the effective index term. However, since the difference in the Bragg wavelengths between sensors are very small (about 1–1.4 nm apart in our case), this minor difference may be neglected and the two coefficients can be treated as constants.

2.2. Simultaneous measurement of shrinkage and temperature

The Bragg wavelength shift is influenced by both the physical stress and thermal change of the grating region. In order to measure the shrinkage and temperature simultaneously, these two responses need to be separated and distinguished. This can be accomplished by placing two FBG sensors under an identical situation, with one of them being free and unrestrained. As such, the latter sensor would only experience thermal change. The set of two simultaneous linear equations for these two sensors are given by

$$\begin{aligned}\Delta\lambda_{B1}/\lambda_{B1} &= k_{\varepsilon 1}\Delta\varepsilon + k_{T1}\Delta T,\\ \Delta\lambda_{B2}/\lambda_{B2} &= k_{T2}\Delta T,\end{aligned} \tag{2}$$

where $k_\varepsilon = (1-p_e)$, $k_T = (\alpha+\xi)$, and subscripts 1 and 2 represent the strain and temperature sensors, respectively. Eq. (2) can be expressed in a matrix form as

$$\begin{pmatrix}\Delta\lambda_{B1}/\lambda_{B1}\\ \Delta\lambda_{B2}/\lambda_{B2}\end{pmatrix} = \begin{pmatrix}k_{\varepsilon 1} & k_{T1}\\ 0 & k_{T2}\end{pmatrix}\begin{pmatrix}\Delta\varepsilon\\ \Delta T\end{pmatrix} = \mathbf{K}\begin{pmatrix}\Delta\varepsilon\\ \Delta T\end{pmatrix}, \tag{3}$$

where $\mathbf{K}$ is the 2×2 sensitivity matrix. After solving for the measurand vector on the right hand side by inverting the sensitivity matrix, we obtain

$$\Delta\varepsilon = \frac{1}{k_{\varepsilon 1}}\left(\frac{\Delta\lambda_{B1}}{\lambda_{B1}}\right) - \frac{k_{T1}}{k_{\varepsilon 1}k_{T2}}\left(\frac{\Delta\lambda_{B2}}{\lambda_{B2}}\right), \Delta T = \frac{1}{k_{T2}}\left(\frac{\Delta\lambda_{B2}}{\lambda_{B2}}\right). \tag{4}$$

In practice, although the two sensors are placed under the same environment, they do not necessarily have the same α, because the temperature sensor might not have direct contact with the structure under test or aligned in the direction of the strain field. However, since in optical fibres ξ is the dominant effect (~95% of the observed Bragg wavelength shift [15]) comparing to α, and that ξ is already assumed to be constant. We may assume that $k_{T1} \approx k_{T2}$, and the expression for strain in Eq. (4) becomes

$$\Delta\varepsilon = \frac{1}{k_{\varepsilon 1}}\left(\frac{\Delta\lambda_{B1}}{\lambda_{B1}} - \frac{\Delta\lambda_{B2}}{\lambda_{B2}}\right). \tag{5}$$

This shows that the early-age shrinkage can be obtained by subtracting the fractional Bragg wavelength shift about

its centre wavelength of the normal sensor from that of the free and unrestrained sensor. The temperature change can be obtained directly from the free and unrestrained sensor under the same environment. It should be noted that, when the FBG sensors are embedded into the specimens, the following assumptions are made: (i) The debonding and slippage of interface between the optical fibre and RPC is negligible, which ensures that the strain field of the RPC is directly transferred to the sensors [16–18]. As such, the strain experienced by the sensor equals to the actual strain of the RPC. (ii) The grating region and the optical fibre as a whole do not suffer from deterioration and damage [19]. This ensures the reflected FBG spectral profiles would not be greatly altered, so as not to affect the detection of the sensor signals.

2.3. Sensor interrogation method

In order to operate with the FBG sensors, an interrogation method is required to detect, acquire and process the measurand-induced signal (i.e., Bragg wavelength shift) from each sensor. A tuneable laser (TL) system, comprising a TL and a photodetector module, is used for the sensor interrogation, and the experimental setup is depicted in Fig. 1. The sensors are connected together in series, such that they are multiplexed by means of wavelength division multiplexing (WDM). The TL constantly scans and sends signals of a wide wavelength range (40 nm) to the FBG sensors through a 3 dB fibre-optic coupler. When the laser wavelength is matched to the Bragg wavelength of the sensor, a large resonant signal is reflected back and passed to a photodetector module that is connected to a computer (PC) via a general purpose interface bus (GPIB) cable. The reflected signal is then processed by the PC, and the reflection spectrum (represented in power vs. wavelength) is displayed onto the PC screen. By tracking the shift in the Bragg wavelength of the two sensors placed together (Eqs. (4) and (5)), the shrinkage and temperature can be simultaneously and separately measured. The TL system can resolve a wavelength shift of 1 pm, which corresponds to a strain and temperature resolution of about 1 με and 0.1 °C, respectively.

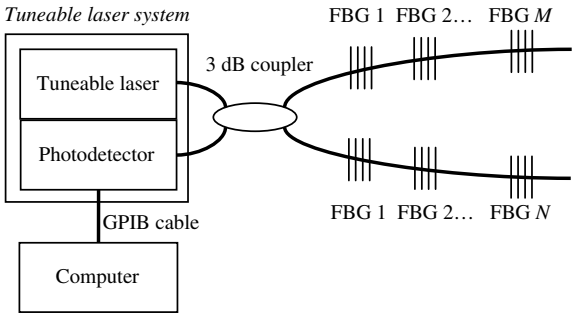

Fig. 1. Schematic diagram of the setup.

3. Experiments

3.1. FBG sensors fabrication

FBG sensors were made at the UNSW FBG-fabrication facility with different Bragg wavelengths using the direct phase-mask technique [20]. The sensors were annealed at high temperature in order to increase the long-term stability, and were re-coated with silicone to protect against mechanical and corrosive damages from the highly alkaline concrete mix. A total of 10 sensors were fabricated with Bragg wavelengths spanned the spectral region between 1520 nm and 1560 nm. The sensors have an average full-width at half-maximum bandwidth of 0.2 nm, and a reflectivity of 99%. The separation between each sensor is about 1–1.4 nm, which corresponds to a measurement range of about 1000 με and 50 °C for strain and temperature, respectively.

3.2. FBG sensors installation

Before casting the RPC mix into the moulds, each FBG sensor was inserted horizontally through the centre of, and parallel to, the mould, as shown in Fig. 2. The sensors for strain measurements were simply placed inside the moulds to have direct contact with the mix, whereas the sensors for temperature measurements were placed inside stiff plastic tubes to isolate from contacting the mix. As such, the temperature sensors were not under the influence of the volume change of the RPC, and were able to monitor the temperature change inside the specimens. Each mould was then covered with a hard plastic sheet folded in triangular shape. This was to help prevent breaking the sensor while pouring the RPC mix, as the sensor was very fragile. The sensors were then spliced together serially in two separate fibre links, and were connected to the TL system for monitoring once the specimens were prepared.

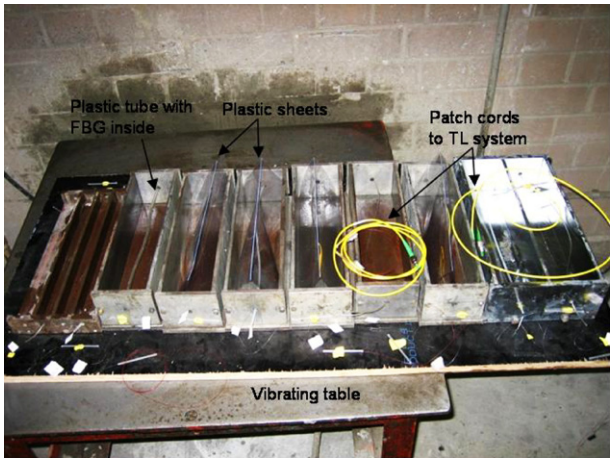

Fig. 2. FBG sensor installation before casting.

3.3. RPC specimens preparation and measurement

The RPC specimens were prepared with a mix proportion given in Table 1, adopted from Gowripalan et al. [21]. All the ingredients were mixed by a drum mixer for about 20 min before adding the water and superplasticiser, which was then mixed for a further 5 min. During the mixing process, the mix was very dry according to the adopted proportion; therefore, additional water was used during the mixing and the actual proportion (by weight) became 210. The mix yielded a water-to-cement (w/c) ratio of 0.31, and a water-to-binder (cement, silica fume) ratio of 0.24. The moulds were placed onto a vibrating table, and were sprayed with oil to reduce the friction at the interface between the moulds and RPC mix. Two sizes of rectangular prismatic mould were used in order to investigate the size effect of the RPC. The dimensions for the standard and mini-prisms were $75 \times 75 \times 280$ mm and $25 \times 25 \times 280$ mm, respectively. In addition, three cylinders with dimensions of 100 mm in diameter and 200 mm in height were also prepared for compression tests.

When the RPC mix was ready, it was poured into the moulds while having the vibrating table turned on. This allowed the mix to be evenly distributed and filled within the moulds. It also provides compaction and removal of voids, so the FBG sensors bond better. During the pouring the folded plastic sheets were lifted up slowly. By doing so, the mix filled up the moulds slowly, so as not to damage the FBG sensors and move their positions. Once the RPC specimens were cast, they were transported and stored in a controlled room with a constant temperature of 20 °C and relative humidity of 50%. All the specimens were remained in the moulds in order to maintain consistent drying conditions and surface exposure areas throughout the whole measurement period. The shrinkage and temperature were monitored immediately after the FBG sensors were connected to the TL system. The final setup inside the controlled room is shown in Fig. 3. Since the time lag between the moment after casting and the time to start taking measurements was small (about 5 min), it was considered as starting time of the measurements. The TL system is capable of taking measurements for all of the FBG sensors together automatically and continuously, at a rate of one reading every 20 s. However, in our experiments, it was set to acquire and record the data once every 2 min, and the data was transmitted to the PC for processing and analysis.

Table 1
RPC mix proportion for a 1 m^3 specimen

Material	Brand	Type/grade/size	Proportion (by weight)
Cement	Portland	GP	680
Silica fume	Tasmanian silica	–	204
Silica flour	Unimin	300G	204
Sand	Sydney	Fine	974
Steel fibres	BHP	186 EE mild steel, 18 mm enlarged ends	156
Superplasticiser	Degussa	Glenium 51	44
Water	–	–	150 (210 in actual mix)

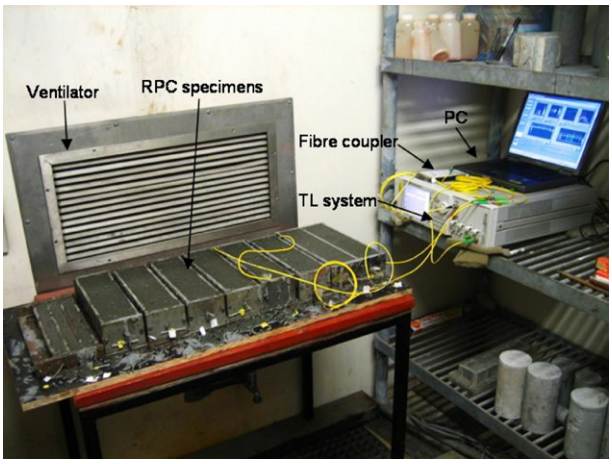

Fig. 3. Final experimental setup inside a temperature and humidity controlled room.

4. Results and discussion

4.1. Compressive strength

At the age of 7 and 28 days from casting, the compressive strength of the RPC was tested using a hydraulic compression testing machine (Instron SATEC 600RD). Their respective strengths were 78.8 MPa and 109.8 MPa, which were lower than the expected strength (~150 MPa). The reasons are: (i) The mix proportion was slightly different from the original. Additional water was used, which gives a larger w/c ratio and hence lesser strength than expected. Also, a different grade of silica flour and type of steel fibres were used. (ii) The mix was intended to be cured by hot-water or steam treatment at a temperature of 90 °C in order to achieve the desired strength. However, in our experiments the specimens were untreated and cured only by drying at room temperature. This can lead to a reduction of strength by as much as 60–70% [22]. (iii) The cylinders were only demoulded at the age of 7 days. As such, only the top surface was fully exposed to the environment, making the water evaporation rate considerably lower which resulted in a lower strength. (iv) Test cylinders were not capped with mortar when performing the compression test, and although the surfaces of both ends were ground, there may still be some irregularities. These irregularities may lead to localised concentrations of stress which would enhance cracking, leading to a lower strength.

4.2. Shrinkage and temperature at early-age

The shrinkage and temperature change of the RPC in the first 24 h after casting are shown in Figs. 4 and 5.

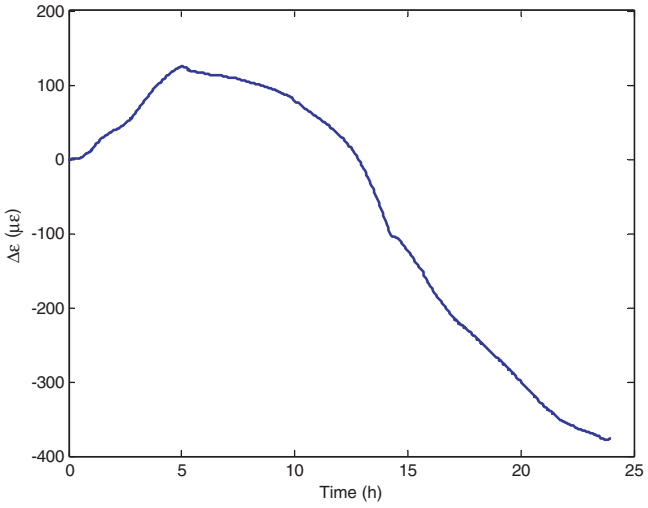

Fig. 4. Shrinkage of RPC at early-age.

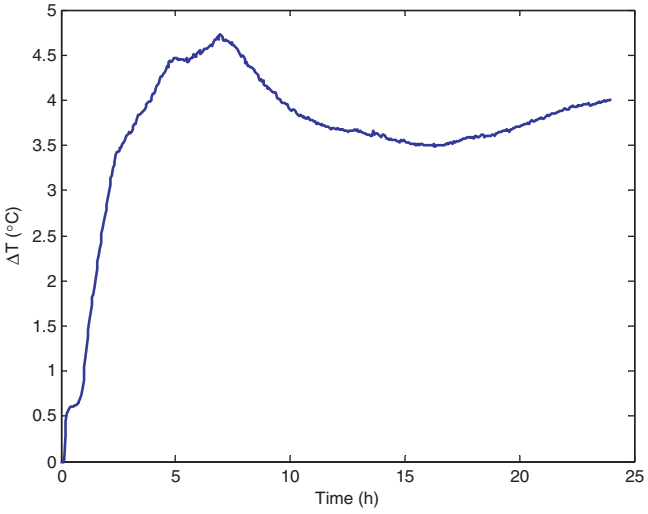

Fig. 5. Temperature change of RPC at early-age.

The RPC remained unchanged in the first 30 min, possibly because the mix was not stiff enough to transfer the strain field to the FBG sensors. At the same time the temperature inside the RPC kept increasing with a momentary slowing down. Then, the RPC started to expand steadily in the initial set due to the absorption of water during the hydration of cement, and the increase in temperature. Since hydration is an exothermic reaction that occurs during setting, it releases heat and causes the temperature of the mix to rise. Thus, a sharp increase in temperature is observed. At about 5 h from casting, the expansion came to its peak value of about 125 με, with the temperature increased by almost 4.5 °C. After that, the RPC started to shrink monotonically at a rapid rate to 377 με after 24 h. This early-age shrinkage accounts for 77% of the overall 7 days shrinkage (488 με). At the same time, the temperature behaved differently from the strain. It first climbed to a peak of 4.7 °C at about 7 h and then dropped down by 1.2 °C at about 16 h before slowly increasing up again. From the temperature curve, the final setting time was when the temperature reached the maximum [23], and that was at about 7 h after casting. This shows that the final setting time does not necessarily correspond to the beginning of shrinking.

4.3. Shrinkage and temperature up to the age of 7 days

The measurements were extended to 7 days from casting, and Figs. 6 and 7 show the shrinkage and temperature change, respectively. From Fig. 6, after shrinking rapidly in the first day, the RPC momentarily reversed to expand again at about 35 h. This is due to the second temperature increase and the renewed reaction of cement components during this period. Although this second peak was comparable to the first one, the amount of expansion due to it was considerably smaller. This is because the RPC was already in its hardened state, and its influence by temperature

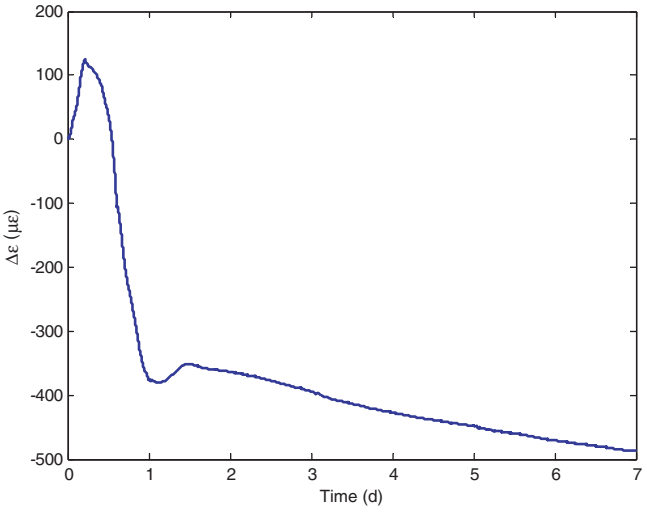

Fig. 6. Shrinkage of RPC for 7 days.

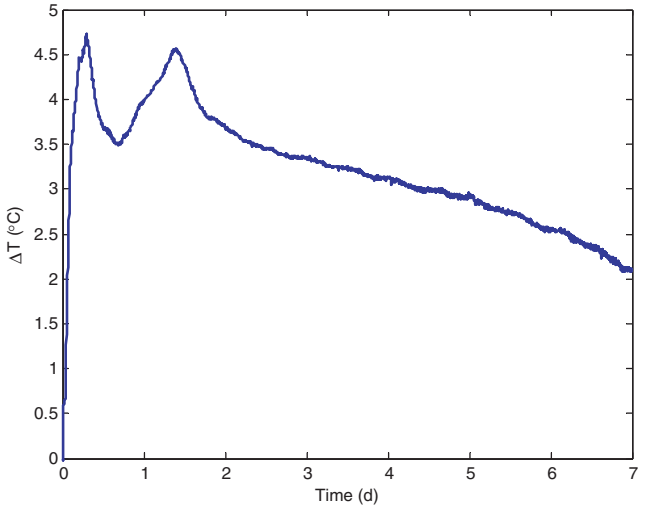

Fig. 7. Temperature change of RPC for 7 days.

would be much smaller than when it was still in the plastic stage. The RPC shrank steadily since the second expansion at a slower rate to 488 με after 7 days. The shrinkage after the early-age to the end of the 7th day was about 23% of the overall 7 days shrinkage. The shrinkage following the setting was mainly due to drying and self-desiccation. In a low w/c ratio concrete like RPC, autogenous shrinkage becomes significant, and may contribute to the overall shrinkage as much as the drying shrinkage does. From Fig. 7 we can see there is a double peak in the temperature curve, one appeared at about 7 h and the other at about 34 h after casting. This double rise in temperature is also observed in normal concrete [24]. While the first peak was due to hydration of cement and setting, the second peak was related to the exhaustion of gypsum and a renewed reaction of cement components (mainly C_3A). The rate of this renewed hydration was slower than the previous hydration, and thus the second peak appeared to have a wider width and the reaction spanned a longer period. From the second day onwards, the temperature decreased monotonically and steadily by about 2.1 °C, which was about half the peak temperature reached during setting.

The relationship between the shrinkage and temperature change is shown in Fig. 8, as a three-dimensional (3-D) line graph plotted as a function of time. It shows that there is an interplay between the shrinkage and temperature, in which they evolved and correlated reasonably well to each other as expected in general. That is, in the first day the RPC expands and temperature increased during the setting. When the RPC is set, it starts to shrink and cool down. The second temperature rise at around 1.5 days after casting caused the specimen to expand again, but to a lesser extent because the specimen is hardened. After that, both the strain and temperature decrease steadily and almost linearly with time to the end of the measurement period. It is expected that the shrinkage will continue to increase at a decreasing rate, while the temperature will eventually reach equilibrium with the ambient temperature.

4.4. Size effect of specimen

The size and shape of the specimen have an indirect influence on the shrinkage at early-age, most notably by the rate of water loss during hydration and drying (soon after the mix is hardened) through the exposed surface areas of the specimen. In our experiment, two sizes of specimen, standard and mini-prisms, were tested and their respective volume-to-surface (exposed surface area) or V/S ratios were 75 mm and 25 mm. Since it is known that the higher the V/S ratio, the lower the shrinkage; so it is expected that mini-prisms would have a larger (and also faster rate) of shrinkage than standard prisms. Figs. 9 and 10 show the shrinkage and temperature change of the RPC specimen of two different sizes. From the shrinkage curve, we observe that the mini-prisms have a smaller expansion than the standard prisms. The expansion occurred at an earlier time with a lower peak value of 25 με at around 2 h after casting. Then, it shrank rapidly up to 7 h, and after that, there is a period of several hours in which it stopped shrinking suddenly and stayed constantly at about 276 με. This is due to the renewed reaction as in the case of standard prism, but occurred at earlier time (almost by half of the time). This reaction can also be seen in the corresponding period in the temperature curve (Fig. 10), which exhibited a rise in temperature. After that, the mini-prism continued to shrink at approximately the same rate as before, until it started to slowly expand again at about 1 day from casting, which lasted for about 1.5 days. This is possibly due to a further exhaustion of gypsum and renewed reaction from the residual cement components that were unused in the previous reaction. But since the amount of residual cement components is much less, the duration of the reaction takes longer. After this final expansion, the shrinkage increased steadily and monotonically until the end of the measurement period.

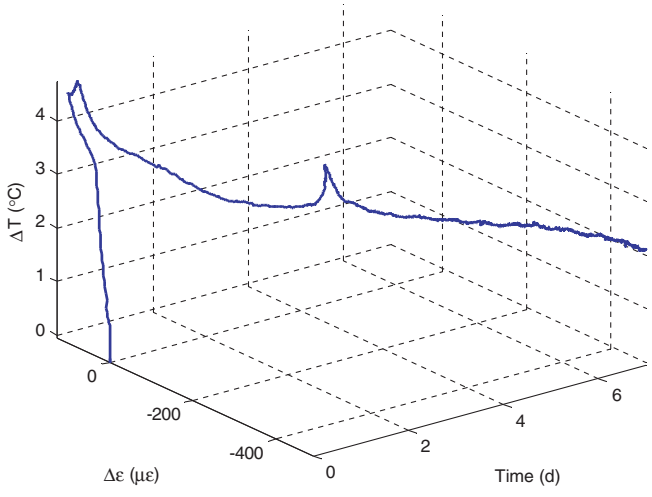

Fig. 8. 3-D line plot of shrinkage and temperature change of RPC as a function of time.

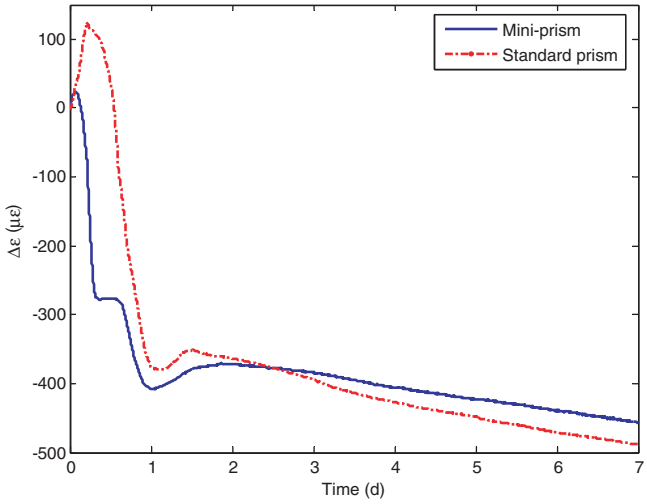

Fig. 9. Shrinkage of RPC of two different sizes for 7 days.

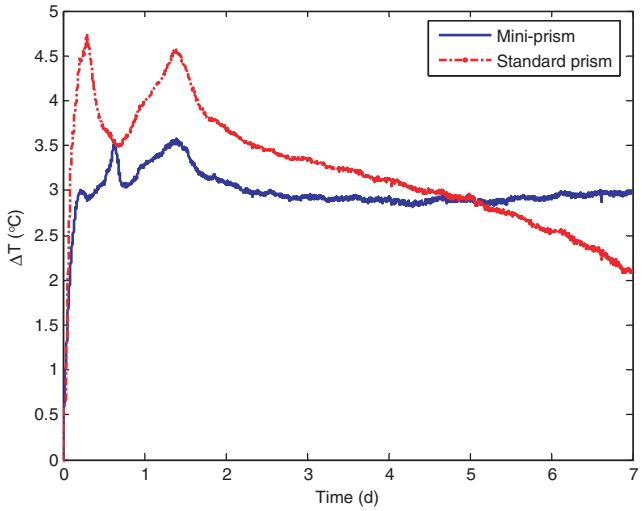

Fig. 10. Temperature change of RPC of two different sizes for 7 days.

At early-age, the mini-prism has a larger overall shrinkage as expected. However, from the second day onwards, the standard prism was observed to have slightly larger shrinkage than the mini-prism. From Fig. 3, we can see that the standard prisms were placed closer to the ventilator than the mini-prisms where there was a large air current flowing through them, and so they experienced faster drying and higher rate of shrinkage.

5. Conclusions

The physical properties of RPC at early-age (the first 24 h from casting) were investigated experimentally using a fibre-optic sensors technique which consists of a TL system and FBG sensors. The FBG sensors provided a relatively simple and reliable way of measuring the early-age characteristics of the RPC, especially the capability of taking measurements for a large number of specimens together simultaneously via WDM. In our experiments, a total of 10 FBG sensors were fabricated and multiplexed together along two optical fibre links. Both the shrinkage and temperature change were monitored continuously at the same time inside a controlled room, immediately after casting and up to 7 days. Results showed that the overall shrinkage for 7 days was 488 με, with the early-age shrinkage contributing about 77% of this. The temperature curve exhibited a double peak behaviour, with a maximum increase of 4.7 °C at about 7 h from casting, which was the final setting time of the RPC. The temperature then declined steadily to 2/3 of the initial increase above the ambient temperature after 7 days. There is an interplay between the shrinkage and temperature, and the evolution of these two parameters with time correlated reasonably well to each other. The specimen size effect was also investigated, which showed that mini-prisms have a higher overall shrinkage and lower temperature change than standard prisms. Further research will be carried out to investigate the autogenous shrinkage, as well as the hydration process of RPC at early-age and for long-term behaviour. This can be accomplished by a method similar to that employed in the present study.

Acknowledgements

The authors would like to thank William Terry for his helpful suggestions. This work was supported in part by the Australian Research Council and the Roads and Traffic Authority, NSW, Australia, under the ARC's Linkage funding scheme (project number LP0347804).

References

[1] Richard P, Cheyrezy MH. Reactive powder concretes with high ductility and 200–800 MPa compressive strength. In: American concrete institute spring convention, ACI SP144-24, San Francisco, March 1994. p. 507–18.
[2] Richard P, Cheyrezy M. Composition of reactive powder concretes. Cem Concr Res 1995;25:1501–11.
[3] Adeline R, Lachemi M, Blais P. Design and behaviour of the Sherbrooke footbridge. In: Proceedings of the international symposium on high-performance and reactive powder concretes, Sherbrooke, August 1998.
[4] Cavill B, Chirgwin G. The world's first RPC road bridge at Shepherds Gully Creek, NSW. In: 21st Biennial conference of CIA, Brisbane, July 2003.
[5] Hajar Z, Simon A, Lecointre D, Petitjean J. Construction of the first road bridges made of ultra-high-performance concrete. In: Proceedings of the 2003 international symposium on high performance concrete, Orlando, October 2003.
[6] Feylessoufi A, Cohen Tenoudji F, Morin V, Richard P. Early age shrinkage mechanisms of ultra-high-performance cement-based materials. Cem Concr Res 2001;31:1573–9.
[7] Morin V, Cohen Tenoudji F, Feylessoufi A, Richard P. Evaluation of the capillary network in a reactive powder concrete during hydration process. Cem Concr Res 2002;32:1907–14.
[8] Krauss M, Hariri K. Determination of initial degree of hydration for improvement of early-age properties of concrete using ultrasonic wave propagation. Cem Concr Compos 2006;28:299–306.
[9] Boumiz A, Vernet V, Cohen Tenoudji F. Mechanical properties of cement pastes and mortars at early ages. Adv Cem Based Mater 1996;3:94–106.
[10] Loukili A, Chopin D, Khelidj A, Le Touzo JY. A new approach to determine autogenous shrinkage of mortar at an early age considering temperature history. Cem Concr Res 2000;30:915–22.
[11] Lacouture JC, Johnson PA, Cohen Tenoudji F. Study of critical behavior in concrete during curing by application of dynamic linear and nonlinear means. J Acoust Soc Am 2003;113:1325–32.
[12] Habel WR, Hofmann D, Hillemeier B. Deformation measurements of mortars at early ages and of large concrete components on site by means of embedded fiber-optic microstrain sensors. Cem Concr Compos 1997;19:81–102.
[13] Glisic B, Simon N. Monitoring of concrete at very early age using stiff SOFO sensor. Cem Concr Compos 2000;22:115–9.
[14] Slowik V, Schlattner E, Klink T. Experimental investigation into early age shrinkage of cement paste by using fibre Bragg gratings. Cem Concr Compos 2004;26:473–9.
[15] Kersey AD, Davis MA, Patrick HJ, LeBlanc M, Koo KP, Askins CG, et al. Fiber grating sensors. J Lightwave Technol 1997;15:1442–63.
[16] Ansari F, Yuan L. Mechanics of bond and interface shear transfer in optical fiber sensors. J Eng Mech 1998;124:385–94.

[17] Leung CKY, Wang X, Olson N. Debonding and calibration shift of optical fiber sensors in concrete. J Eng Mech 2000;126:300–7.
[18] Li Q, Li G, Wang G, Ansari F, Liu Q. Elasto-plastic bonding of embedded optical fiber sensors in concrete. J Eng Mech 2002;128: 471–8.
[19] Habel WR, Polster H. The influence of cementitious building materials on polymeric surfaces of embedded optical fibers for sensors. J Lightwave Technol 1995;13:1324–30.
[20] Hill KO, Malo B, Bilodeau F, Johnson DC, Albert J. Bragg gratings fabricated in monomode photosensitive optical fiber by UV exposure through a phase mask. Appl Phys Lett 1993;62:1035–7.
[21] Gowripalan N, Watters R, Gilbert RI, Cavill B. Reactive powder concrete (RPC) for precast structural concrete – research and development in Australia. In: 21st Biennial conference of CIA, Brisbane, July 2003.
[22] Dallaire E, Aitcin P, Lachemi M. High-performance powder. ASCE Civ Eng Mag 1998(January):48–51.
[23] Neville AM, Brooks JJ. Concrete technology. revised ed. Harlow: Prentice Hall; 2004.
[24] Neville AM. Properties of concrete. 4th ed. Essex: Longman; 1995.